

1  
2  
3 **Paste Ageing Spontaneously Tunes TiO<sub>2</sub> Nanoparticles into Reproducible**  
4  
5  
6 **Electro-Sprayed Photo-Electrodes**  
7  
8

9 Md. Shahiduzzaman<sup>1,6, \*†</sup>, Boyang Chen<sup>2†</sup>, Md. Akhtaruzzaman<sup>3</sup>, LiangLe Wang<sup>4</sup>, Hiroki  
10 Fukuhara<sup>2</sup>, Koji Tomita<sup>5</sup>, Satoru Iwamori<sup>6</sup>, Jean-Michel Nunzi<sup>1,7</sup>, Tetsuya Taima<sup>1,4</sup>, and  
11  
12  
13  
14 Shinjiro Umezu<sup>2\*</sup>  
15

16  
17 <sup>1</sup>*Nanomaterials Research Institute (NanoMaRi), Kanazawa University, Kakuma, Kanazawa*  
18 *920-1192, Japan*  
19

20  
21 <sup>2</sup>*Department of Modern Mechanical Engineering, Waseda University, 3-4-1 Ookubo,*  
22 *Shinjuku-ku, Tokyo, 269-8555 Japan*  
23

24  
25 <sup>3</sup>*Solar Energy Research Institute, The National University of Malaysia, 43600 Bangi,*  
26 *Selangor, Malaysia*  
27

28  
29 <sup>4</sup>*Graduate School of Frontier Science Initiative, Kanazawa University, Kakuma, 920-1192*  
30 *Kanazawa, Japan*  
31

32  
33 <sup>5</sup>*Department of Chemistry, School of Science, Tokai University, Kitakaname, Hiratsuka 259-*  
34 *1292, Japan*  
35

36  
37 <sup>6</sup>*Research Institute of Science and Technology (RIST), Tokai University, Kitakaname,*  
38 *Hiratsuka 259-1292, Japan*  
39

40  
41 <sup>7</sup>*Department of Physics, Engineering Physics and Astronomy, Queen's University, Kingston*  
42 *K7L-3N6, ON, Canada*  
43

44  
45  
46  
47 *†Contributed equally to this work*  
48

49  
50  
51 Tel / Fax: +81-76-234-4937  
52

53  
54 \*E-mail: shahiduzzaman@se.kanazawa-u.ac.jp; umeshin@waseda.jp  
55  
56  
57  
58  
59  
60

## Abstract

In this study, the spontaneous microstructure tuning of TiO<sub>2</sub> was observed by ageing the ethanol/water TiO<sub>2</sub> paste for up to 20 days at ambient conditions. A dynamic light scattering study reveals that it formed the outstanding reproducible TiO<sub>2</sub> microstructure with ~ 200 nm average particle size and stabilizes in 6 to 20 days under ambient atmosphere. Interestingly, as deposited day-15 sample spontaneously changed its crystallinity upon keeping the paste at ambient conditions, meanwhile the day 0 sample showed an amorphous structure. A dense, uniform and stable TiO<sub>2</sub> electrode was cast on FTO-substrate using the electro-spray-technique. We exploit the spontaneous evolution of the TiO<sub>2</sub> nano-powder to revisit the fabrication procedure of the TiO<sub>2</sub> photoelectrode for dye-sensitized solar cells (DSSCs). The controlled microstructure TiO<sub>2</sub> film was used in DSSCs, which to the best of our knowledge, achieved the highest power conversion efficiency of 9.65% using N719 dye to sensitize the TiO<sub>2</sub> photoanode.

Keywords: Electro-spray-technique; Spontaneous microstructure tuning; TiO<sub>2</sub>; ageing; reproducible; N719 dye; dye-sensitized solar cells.

## 1. Introduction

Titanium dioxide (TiO<sub>2</sub>) is a durable photocatalyst and is also a multifunctional material owing to its diverse applications in paints, sunscreens, water purification, self-cleaning, hydrogen storage, anti-viral, antiseptic, anti-odor, bio-medical ceramic and implanted biomaterials, antimicrobial plastic packaging, and photovoltaic technologies.<sup>1-5</sup> Its three distinct crystalline polymorphs are anatase (tetragonal), brookite (orthorhombic), and rutile (tetragonal), which are obtained depending on the synthesis process, the parameters and conditions.<sup>6, 7</sup> Their opto-electronic behaviors, transmittance, stability and catalytic efficiency

1  
2  
3 depend on a wide range of variables, like surface morphology, particle size, shape, ratio of  
4 anatase/rutile and crystal orientation.<sup>8</sup> TiO<sub>2</sub> nanostructures with large surface area, high  
5 electron mobility and efficient light scattering capability are highly desired for improved  
6 photovoltaic performances. The optimal parameters of a specific dye-sensitized solar cell  
7 (DSSCs) significantly depend on the dye and photoanode characteristics. Many studies were  
8 carried out on the development of dyes and photoanodes in order to further improve the device  
9 efficiency and stability.<sup>9, 10</sup> Recently, doping of non-metal and metal ions has been widely  
10 investigated to moderate or reduce the optical band gap by introducing the intermediate energy  
11 levels in the host TiO<sub>2</sub>, resulted in efficiently electron flows. Bhorde and colleagues<sup>11</sup> reported  
12 DSSCs with PCEs of 1.31 to 6% by using varying doped -TiO<sub>2</sub> nanocrystals. J. Liu et al.<sup>12</sup>  
13 synthesized TiO<sub>2</sub> NPs by using a simple one-step hydrothermal method and applied it to  
14 DSSCs, followed by achieving a PCE of 8.34%. Thus, the choice of a photoanode material and  
15 its microstructure has significant importance for DSSCs. It determines the photovoltaic  
16 parameters by enabling light scattering/absorption for efficient light harvesting.<sup>13</sup> Therefore,  
17 the choice of a deposition technique for the TiO<sub>2</sub> nanostructure is critical to enable large  
18 production volumes, versatility, low energy consumption and so on.<sup>14</sup> Several deposition  
19 techniques were developed, including sol-gel,<sup>15-17</sup> chemical vapor deposition,<sup>18, 19</sup>  
20 hydrothermal,<sup>20</sup> solvothermal,<sup>21</sup> microwave,<sup>22</sup> electrochemical oxidation,<sup>23</sup> electrospinning,<sup>24</sup>  
21 spray-pyrolysis,<sup>25</sup> chemical bath,<sup>26</sup> sputtering,<sup>27</sup> atomic layer deposition,<sup>28</sup> oblique electrostatic  
22 inkjet,<sup>29</sup> and electrostatic inkjet-(EI),<sup>30</sup> to fabricate TiO<sub>2</sub> photoanodes. The commonly used sol-  
23 gel technique enables TiO<sub>2</sub> nanostructure production but is limited in large-scale production.  
24 Chemical vapor deposition (11) and sputtering<sup>27</sup> require a vacuum environment and suffer a  
25 slow deposition rate. Scalable bottom-up atomic layer deposition<sup>28</sup> requires relatively long  
26 processing times and is rather expensive also. Moreover, most of these methods must be carried  
27 out under high energy demanding and/or high-temperature conditions, in order to properly  
28  
29  
30  
31  
32  
33  
34  
35  
36  
37  
38  
39  
40  
41  
42  
43  
44  
45  
46  
47  
48  
49  
50  
51  
52  
53  
54  
55  
56  
57  
58  
59  
60

1  
2  
3 control the required nanostructure, especially hierarchical nanostructures combining the  
4 desired morphology, size, thickness and porosity. Therefore, the precise tuning of TiO<sub>2</sub>  
5 nanoparticles and thin-films preparation protocols using a cost-effective micro- and nano  
6 fabrication technique has become a significant challenge.  
7  
8  
9

10  
11  
12 In this study, we investigated the spontaneous microstructure tuning of TiO<sub>2</sub> by ageing  
13 the ethanol/water TiO<sub>2</sub> paste up to 20 days at ambient conditions. Interestingly, the Gibbs-  
14 energy driven process yields a very small dispersion in the mean diameter of the TiO<sub>2</sub> NPs  
15 prepared within day 6 to day 20, with outstanding reproducibility and stability over five  
16 samples (15% ethanol in water paste). Out of this, a dense, uniform and stable TiO<sub>2</sub> film was  
17 fabricated on FTO-substrate by using a simple, green, low-cost and easily controllable electro-  
18 spray technique. Our electro-spray (ES) process offers a simple, cost-effective, and promising  
19 way to obtain high-quality TiO<sub>2</sub> films with an easy-to-control thickness as well as a high  
20 reproducibility. To the best of our knowledge, the controlled microstructure TiO<sub>2</sub> film enabled  
21 a DSSCs that achieved the highest power conversion efficiency of 9.65% using the N719 dye  
22 sensitization of a TiO<sub>2</sub> photoanode prepared under ambient conditions.  
23  
24  
25  
26  
27  
28  
29  
30  
31  
32  
33  
34  
35  
36

## 37 **2. Experimental Section**

### 38 **2.1 Materials**

39  
40  
41 All materials were purchased from commercial suppliers and were used without further  
42 purification. Fluorine doped-tin oxide (FTO)-patterned glass substrates were purchased from  
43 AXEL (Tokyo, Japan). P25 particle was purchased from Evonik-Japan (Tokyo, Japan).  
44 Acetylacetone was bought from TCI (Tokyo, Japan). N719 dye (PECD07) was purchased from  
45 Peccell (Tokyo, Japan). Dimethyl propylimidazolium was purchased from Shikoku Chemicals  
46 Corporation (Kagawa, Japan). Acetonitrile and *t*-Butyl Alcohol were bought from Wako Pure  
47 Chemical (Osaka, Japan). Lithium iodide, iodine ACS reagent, triton-X, polyethylene glycol,  
48  
49  
50  
51  
52  
53  
54  
55  
56  
57  
58  
59  
60

1  
2  
3 and guanidine thiocyanate were purchased from Sigma-Aldrich (St. Louis, Missouri; United  
4 States).  
5  
6

## 7 8 **2.2 Preparation of TiO<sub>2</sub> Paste**

9  
10 P25 particles were used to prepare the TiO<sub>2</sub> paste. P25 particles (11.1g) were dissolved  
11 into ethanol (15% mol/L; 36mL) followed by stirring at 1500 rpm for 360 s and defoaming at  
12 2000 rpm for 60 s. Since then, acetylacetone (1.2 mL), triton-X (30%; 6 mL) and polyethylene  
13 glycol (1.1g) were sequentially added to the solution with further stirring and defoaming.  
14  
15  
16  
17  
18  
19

## 20 21 **2.3 Preparation of N719 Dye Solution**

22  
23 Acetonitrile (20 mL) and *t*-butyl alcohol (20 mL) were added into a screw tube bottle,  
24 followed by adding N719 dye (0.02377 g) and sonication for 10 to 20 minutes.  
25  
26  
27

## 28 29 **2.4 Preparation of Electrolyte Solution**

30  
31 *t*-butyl pyridine (0.0676 g) was added to a 6 cc screw vial through a Pasteur pipette.  
32 Dimethyl propylimidazolium (0.1596 g), lithium iodide (0.0133 g), iodine (0.0127 g), and  
33 guanidinium isocyanate (0.0118 g) were then added. The precursor solution was filled up to 1  
34 mL with acetonitrile using a Pasteur pipette followed by heating at 30 °C to make the  
35 electrolyte solution.  
36  
37  
38  
39  
40  
41  
42

## 43 44 **2.5 Fabrication of TiO<sub>2</sub> Electrodes and Dye-sensitized Solar Cells**

45  
46 The FTO-patterned glass substrates were cut into 16 mm × 22 mm and washed  
47 consecutively with a soap solution, distilled water, acetone, ethyl alcohol, and once more  
48 distilled water. Then, UV ozone treatment was applied to the substrates for 15 min. The TiO<sub>2</sub>  
49 paste was cast onto the substrates by ES-technique. The applied voltage between the nozzle  
50 and the FTO-substrate creates an electric field that provides the power to separate ejected  
51 titania droplets from the nozzle and drive them towards the target. The tip of a Terumo syringe  
52  
53  
54  
55  
56  
57  
58  
59  
60

1  
2  
3 (10 mL) was fitted with a San-ei Tech Ltd (Tokyo, Japan) TT taper nozzle (0.21 mm internal  
4 diameter), and the solution was filled up to 2.0 ml with the as prepared TiO<sub>2</sub> paste. The nozzle  
5  
6 was installed at the end of the tank. To maintain the electric field around the nozzle tip, a holed  
7  
8 plate electrode (outside 100 × 145 mm<sup>2</sup>, hole diameter of 60 mm) was used between the nozzle  
9  
10 tip and the FTO-electrode. The gap between the FTO substrate and the tip of the nozzle was  
11  
12 fixed at 10 mm, and the discharge time was 40 s to 45 s and obtained optimal 30 μm thickness  
13  
14 of TiO<sub>2</sub>. Applied voltage was 8.0 kV. As prepared TiO<sub>2</sub> paste was further dispersed by  
15  
16 sonication for several minutes. After deposition, the substrates were sintered at 500 °C for 30  
17  
18 min in a muffle furnace and allowed to cool down to room temperature. The resultant samples  
19  
20 were used as a photoanode. The TiO<sub>2</sub> nanostructure surface coverage was evaluated for  
21  
22 different deposition conditions based on the duration of the discharge. The TiO<sub>2</sub> electrodes  
23  
24 were sensitized by immersion in an ethanol solution containing 0.5 mM N719 dye solution at  
25  
26 37 °C for 180 minutes in a dark room. The prepared photoanode was assembled with platinum  
27  
28 electrode and iodine electrolyte.  
29  
30  
31  
32  
33  
34  
35  
36  
37

## 38 **2.6 Characterization**

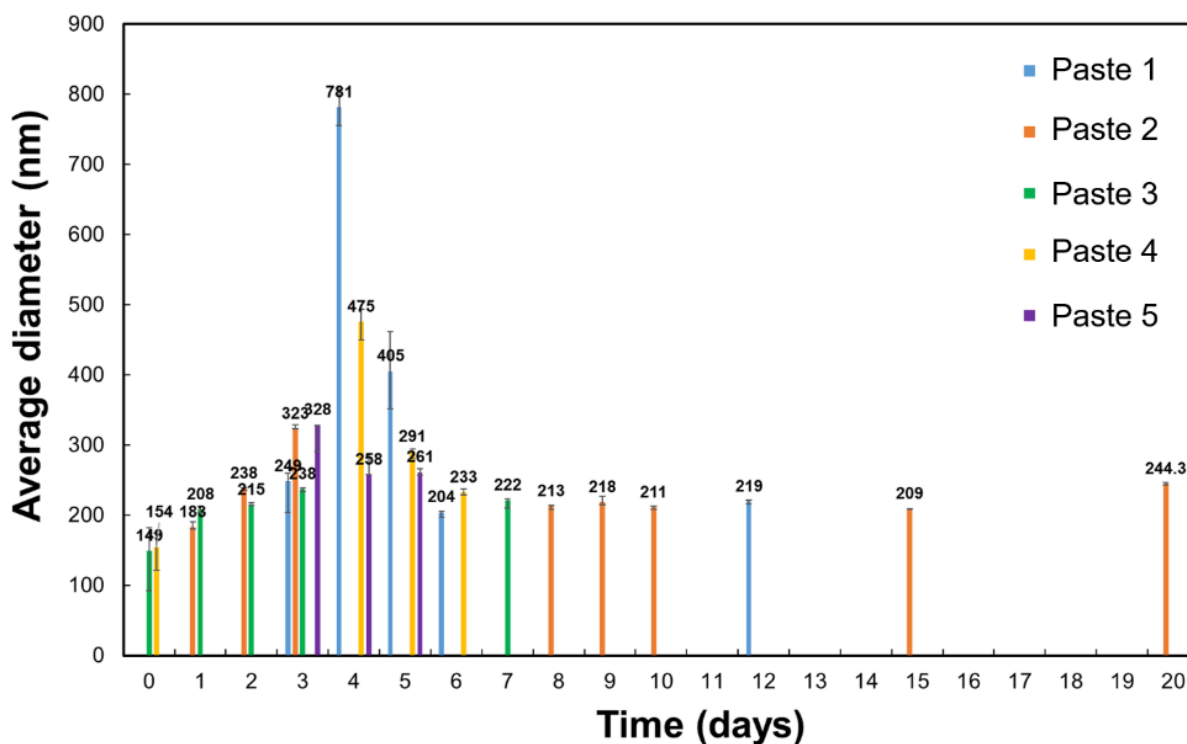
39  
40  
41 The average particle size of the TiO<sub>2</sub> nanostructures was determined by dynamic light  
42 scattering (HORIBA/LB-550, Tokyo, Japan). Field emission scanning electron microscopy  
43 (FE-SEM) (S-4800, Hitachi High-Tech, Tokyo, Japan) was used to examine the microstructure.  
44  
45 The crystalline phase and average pore size of the samples were determined by X-ray  
46  
47 diffraction (XRD) and X-ray reflectometry (XRR) (RINT-Ultima3, RIGAKU, Tokyo, Japan).  
48  
49 UV-vis absorption spectra of the TiO<sub>2</sub> films were recorded using a PerkinElmer/Lamda 650,  
50  
51 (Tokyo, Japan) absorption spectrophotometer. X-ray photoelectron spectroscopy (XPS) of  
52  
53 TiO<sub>2</sub> was analyzed on a JPS-9010 (JEOL Ltd., Japan) with a non-monochromatic Mg Kα  
54  
55 source (photon energy: 1253.6 eV). The current density *versus* voltage (*J–V*) curves were  
56  
57  
58  
59  
60

1  
2  
3 recorded under simulated solar conditions ( $100 \text{ mW}\cdot\text{cm}^{-2}$ , AM 1.5, 1 sun intensity) using a  
4  
5 Keithley 2401 digital source meter. A monochromatic xenon arc light (Bunkoukeiki, SMI-  
6  
7 250JA) was used to measure the incident photon-to-electron conversion efficiency (IPCE) of  
8  
9 the devices. Active area of the devices was  $0.25 \text{ cm}^2$ .

### 13 3. Results and discussion

#### 16 3.1 Spontaneous Micro-tuned $\text{TiO}_2$ Particle Size by $\text{TiO}_2$ Paste Ageing

18 In the first step of this study, dynamic light scattering (DLS) was used to investigate  
19  
20 the  $\text{TiO}_2$  particle size while ageing the  $\text{TiO}_2$  paste at ambient atmosphere for up to 20 days  
21  
22 (Figure 1). The as-prepared  $\text{TiO}_2$  paste contains a large quantity of  $\sim 150 \text{ nm}$ -size aggregated  
23  
24 primary particles. Later, the average particle size gradually increases from 150 to 780 nm and  
25  
26 aggregates between day 1 and day 4. This implies that primary particles are turning into small  
27  
28 and large secondary particles.



56 **Figure 1.**  $\text{TiO}_2$  particle size obtained from dynamic light scattering. Each point represents the  
57 mean  $\pm$  S diameter D. Five pastes prepared under similar conditions were used to determine  
58 the  $\text{TiO}_2$  particle size.  
59  
60

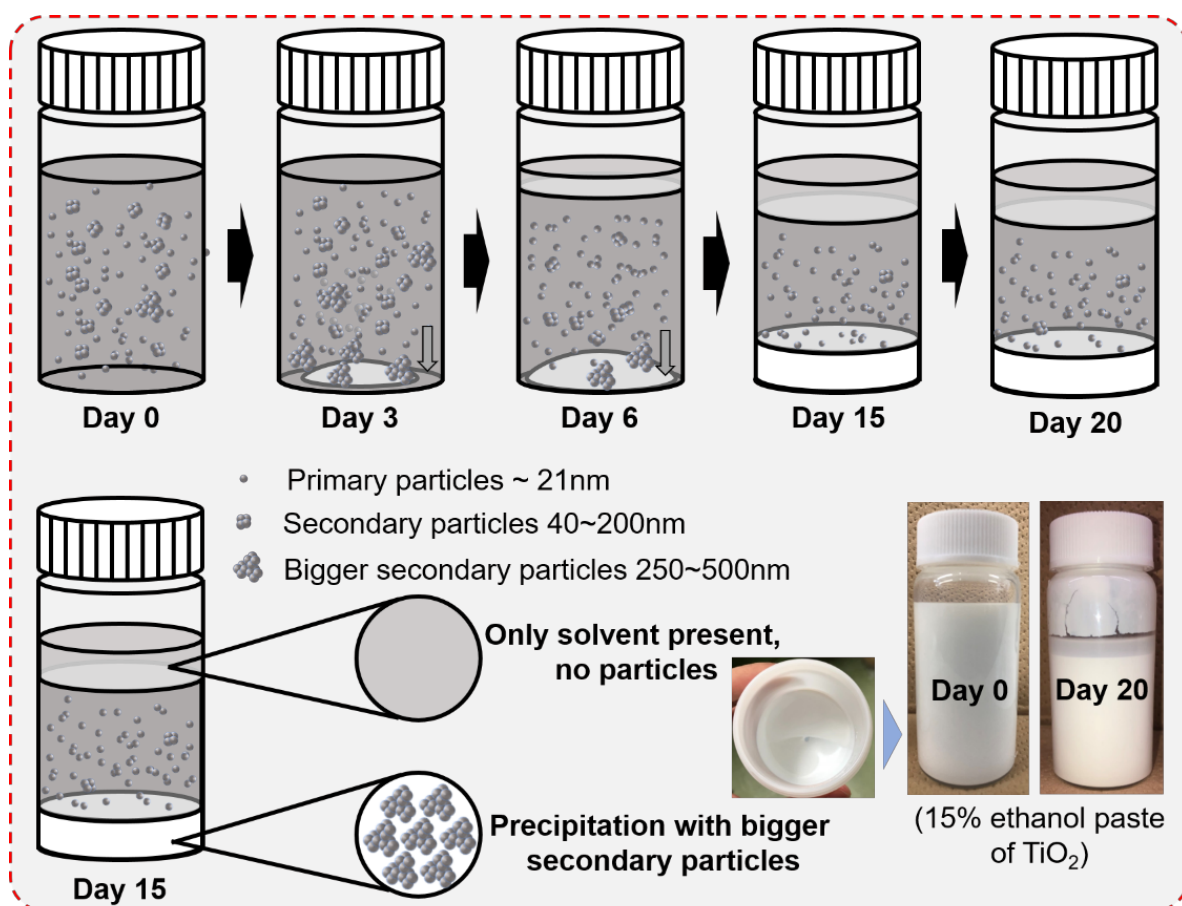


**Figure 2.** Scheme of the spontaneous TiO<sub>2</sub> paste evolution while ageing up to day 20 under ambient atmosphere.

Large aggregated secondary particles precipitate after day 5 and do not show-up anymore in the DLS. The observed average particle size then becomes stable up to day 20 (**Figure 1**). From day 6 on, it can be seen that a particle free solvent layer appears (**Figure 2**), meanwhile the resultant average particle size decreases down to ~ 200 nm and stabilizes. Interestingly, when prepared in day 6 to day 20, we observe a very small dispersion in the mean TiO<sub>2</sub> NP diameter, which indicates outstanding reproducibility over five samples (15% ethanol paste). These results suggest that ageing the TiO<sub>2</sub> paste up to 20 days at ambient atmosphere is a crucial factor to obtain a reproducible TiO<sub>2</sub> particle size.

Spontaneous aggregation and precipitation are common in suspensions of nanoparticles. It can ultimately lead to the formation of a zeolite.<sup>31</sup> Stabilization of the suspended particle size

1  
2  
3 over long ageing periods was observed in TiO<sub>2</sub> suspensions prepared for different applications  
4 like sunscreen emulsions.<sup>32</sup> The phenomenon is named coalescence or coagulation. Youn et  
5 al.<sup>33</sup> calculated the time lag for the agglomeration of the primary particles into a stable  
6 suspension using first principles. In all situations, it was observed that primary particles  
7 coalesce into size-stable low-dispersion nanoparticle suspensions after the time-lag.<sup>34, 35</sup> The  
8 exact stable final size depends on the exact size and concentration of the primary  
9 nanoparticles.<sup>36</sup> The Gibbs-energy driven process<sup>37</sup> has fundamental consequences on the paste  
10 used to fabricate the photoanodes: it yields highly reproducible results once the nano-particle  
11 size has spontaneously stabilized.  
12  
13  
14  
15  
16  
17  
18  
19  
20  
21  
22  
23  
24

### 25 ***3.2 Electro-Spray preparation of a dense, uniform and stable TiO<sub>2</sub> Photoanode***

26  
27 In the second part of this study, the TiO<sub>2</sub> photoanode was patterned by electro-spray.  
28  
29 **Figure 3** shows the electro-spray single nozzle experimental setup for TiO<sub>2</sub> electrode  
30 patterning. ES discharges TiO<sub>2</sub> from the highly viscous liquid paste in the form of a spray via  
31 the electrostatic force in the direction perpendicular to the FTO-glass substrate, resulting in  
32 large droplets stacked into thick film on the substrate (Inset in **Figure 3**).  
33  
34  
35  
36  
37  
38  
39  
40  
41  
42  
43  
44  
45  
46  
47  
48  
49  
50  
51  
52  
53  
54  
55  
56  
57  
58  
59  
60

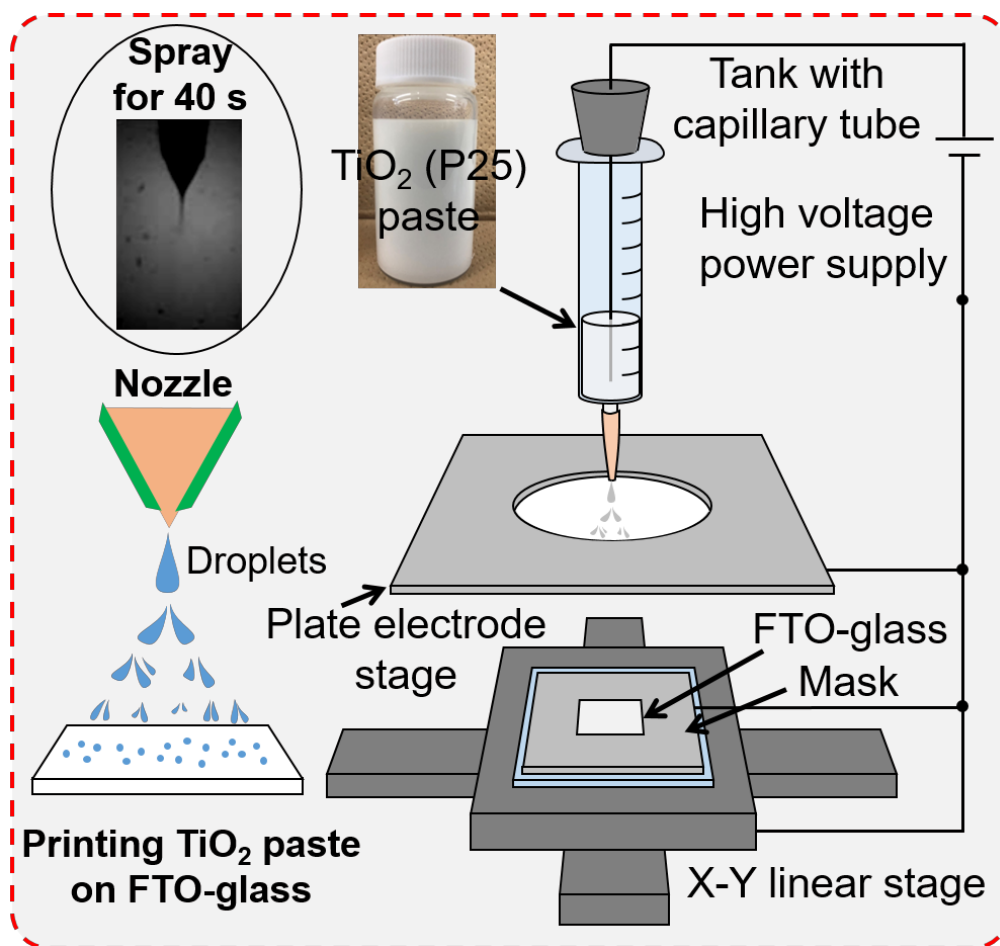


**Figure 3.** Schematic illustration of the electro-spray setup used to pattern the  $\text{TiO}_2$  electrode on the FTO-glass substrate.

On the upper left, the photograph in the center of the illustration shows the drop ejection in the spray mode. Inset shows a photograph of the white  $\text{TiO}_2$  (P25 nanoparticles) precursor paste. A dense and smooth  $\text{TiO}_2$  electrode was patterned to illustrate the single-nozzle electro-spray technique (**video S1**; Supplementary Information).  $\text{TiO}_2$  was precisely deposited under the electrostatic force. electro-spray permits controlled growth of  $\text{TiO}_2$  films by changing the ethanol concentration in the water paste. Control growth of the  $\text{TiO}_2$  microstructure, including particle size has significant importance to improve the DSSCs' performance.

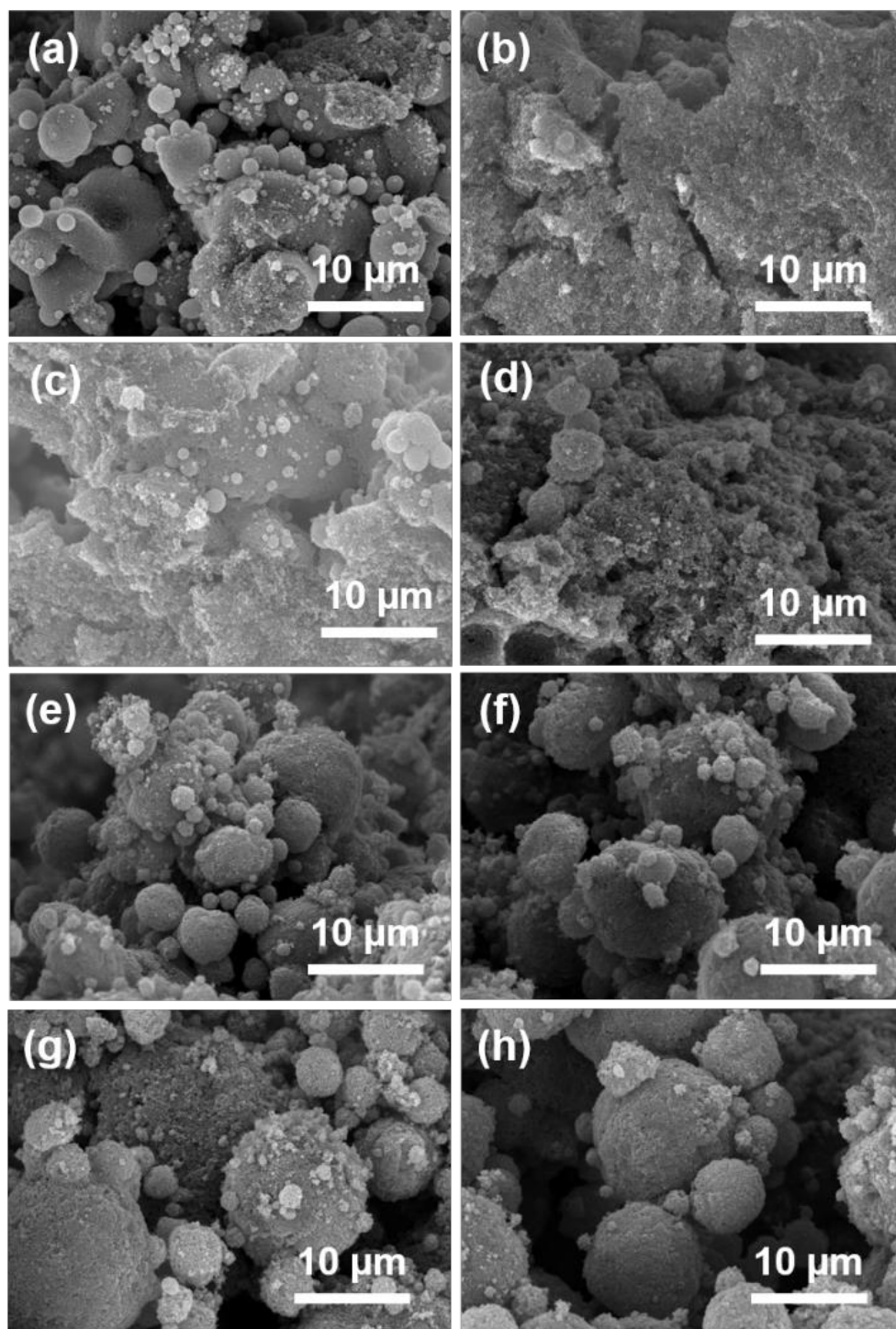


**Figure 4.** Top-view SEM images of TiO<sub>2</sub> porous structure fabricated with varying ethanol percentage of (a) 0, (b) 5, (c) 15, (d) 25, (e) 50, (f) 75, (g) 85, and (h) 99.5% in the water paste.

1  
2  
3 We investigated the effect of 15, 25, 50, 75, 85 and 99.5% ethanol concentration in the  
4 water paste on the pore sizes and microstructure of the electro-spray deposited-TiO<sub>2</sub> films. The  
5 average pore size and microstructure were observed by X-ray reflectivity (XRR) and FE-SEM,  
6 respectively. Controlled growth of a film with 72 nm to 350 nm average pore size was achieved  
7 by adjusting the voltage (8.0 kV) and gap (10 mm) between the nozzle and FTO-substrate  
8 (**Figure S1a**). The pore size of the TiO<sub>2</sub> film depends on the ethanol percentage in the paste.  
9 Increased pore size yields an incomplete film with large voids. **Figure 4a-h** shows the top-  
10 view FE-SEM images of the TiO<sub>2</sub> microstructure with different pore sizes. The FE-SEM  
11 images reveal an aggregated morphology with large voids for 0, 25, 50, 75, 85, 99.5% ethanol  
12 in the water paste, while the morphology is well developed for 5 and 15% ethanol. The pore  
13 size and morphology of the TiO<sub>2</sub> microstructure changes depending on the ethanol  
14 concentration in the water paste. We assume that a large percentage of ethanol in the paste  
15 produces large TiO<sub>2</sub> aggregated scaffolds with large voids, which may affect electron diffusion  
16 and recombination process in the TiO<sub>2</sub> film, resulting in a substantial difference in charge  
17 collection properties.<sup>38</sup> Given that the porosity and microstructure of TiO<sub>2</sub> films from 15%  
18 ethanol paste are within the optimum range regardless of the particle size to provide sufficient  
19 pathways for electrons to travel across the TiO<sub>2</sub> microstructure,<sup>39</sup> we used 15% ethanol in water  
20 as an optimum condition for the systematic study of the spontaneous micro-tuning of electro-  
21 spray deposited TiO<sub>2</sub> electrodes for efficient and reproducible DSSCs application.  
22  
23  
24  
25  
26  
27  
28  
29  
30  
31  
32  
33  
34  
35  
36  
37  
38  
39  
40  
41  
42  
43  
44  
45  
46

47 The evolution of the crystalline phase of the TiO<sub>2</sub> NPs film formed without sintering  
48 was also investigated by XRD on TiO<sub>2</sub> paste aged from 0 to 20 days at ambient atmosphere  
49 (**Figure S1b**). The as-prepared day-0 TiO<sub>2</sub> NPs in the paste is composed of 7.6% rutile and  
50 92.4 % anatase phase. The stabilized TiO<sub>2</sub> NPs evolve into a 27% rutile phase after day 7 and  
51 up to day 20, as shown in the calculated data (**Figure 5a**). Interestingly, the as-deposited-day  
52  
53  
54  
55  
56  
57  
58  
59  
60

15 samples (without sintering) had an increased rutile phase content of 33% (67% anatase) upon ageing the paste at ambient conditions (Figure 5b).

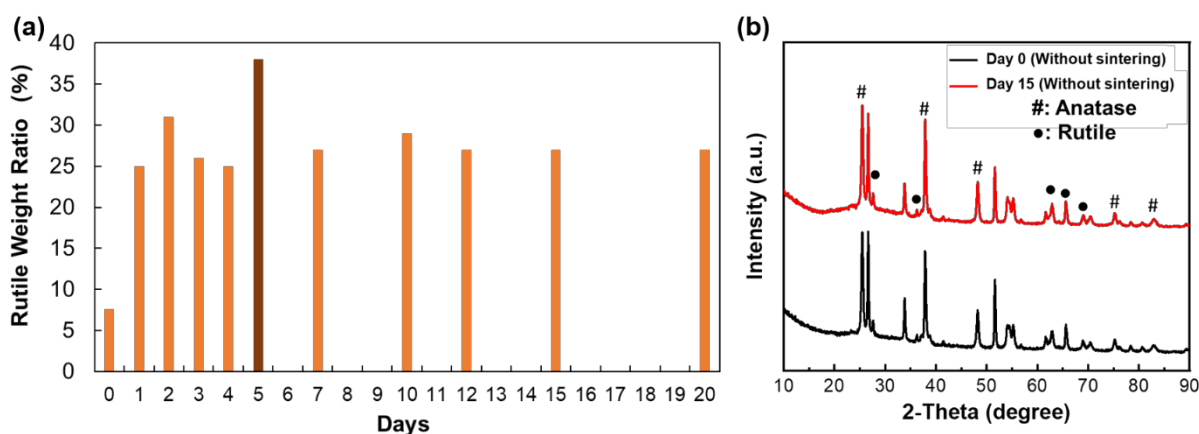


**Figure 5.** XRD spectra after the sintering of (a) TiO<sub>2</sub> film formed with TiO<sub>2</sub> paste aged from 0 to 20 days at ambient atmosphere; and (b) TiO<sub>2</sub> films patterned before sintering on the FTO-substrates for the day 0, and day 15 samples.

It was reported that the rutile phase is the most stable one with lower Gibbs energy (about 10 kJ/mol) at room temperature.<sup>40</sup> Interestingly, for the solar cell application, the index of refraction of rutile is larger than the one of anatase, which consequence is that rutile will scatter more light than the anatase phase.<sup>41</sup> Increased scattering (haze) couples more light into the solar device, which in turn increases the short circuit current in DSSCs, as observed previously.<sup>42</sup> Indeed, scattering efficiency of the photoanode in DSSCs is a key ingredient to the efficiency optimization.<sup>43</sup>

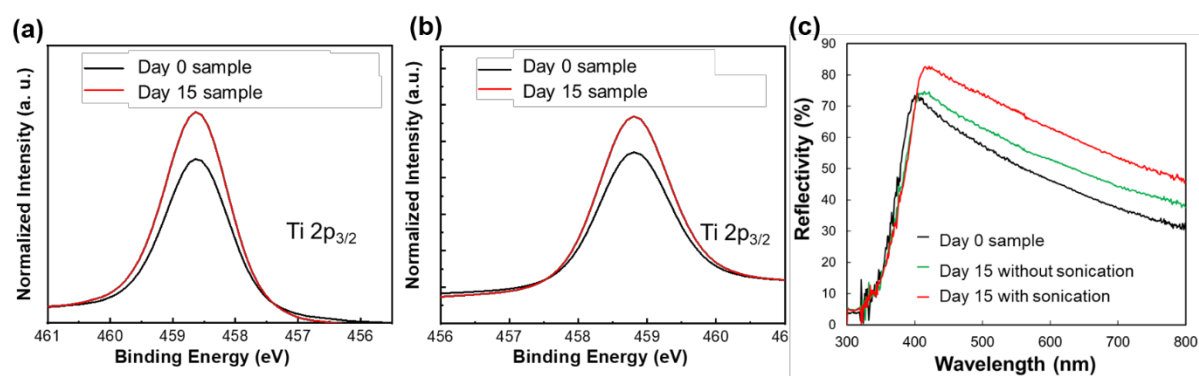


**Figure 6.** XPS spectra of the TiO<sub>2</sub> films formed with day 0, and day 15 of (a) before and (b) after sintering. (c) Reflectance spectra of TiO<sub>2</sub> films on FTO-glass substrates for varying ageing of the paste

1  
2  
3 **Figure 6** shows the XPS spectra of the TiO<sub>2</sub> films formed before and after sintering for  
4 the day 0, and optimum stabilized day 15 samples. The Ti 2p<sub>3/2</sub> peak intensity at 458.7 eV  
5 increased in the day 15 samples compared with day 0 samples, which indicates higher  
6 crystallinity.<sup>44</sup> This confirms the spontaneity of the crystalline evolution of the day 15 samples,  
7 regardless of the heat-treatment. The rutile phase has a lower ionization potential than the  
8 anatase one (7.40 vs. 7.96 eV), which favors a larger open circuit voltage.<sup>45</sup> Although it is  
9 understood that the rutile can be more efficient for the DSSC application than the anatase, it  
10 was also reported that the strong synergistic effect between anatase and rutile TiO<sub>2</sub> phases  
11 significantly enhances the solar cell activity.<sup>46</sup>

12  
13  
14  
15  
16  
17  
18  
19  
20  
21  
22  
23 **Figure 6c** shows the UV-visible diffuse reflectance spectra of the day 0 and day 15  
24 samples (without sintering), with and without sonication. Diffuse reflectance, which is also a  
25 measure of scattering, is lower in the day 0 samples. The absorption band edge of the day 0  
26 TiO<sub>2</sub> sample is slightly blue shifted from the day 15 samples, with and without sonication. This  
27 can be explained by the sample composition (**figure 5a**), anatase indeed has a larger bandgap  
28 (3.2 eV) than rutile (3.0 eV).  
29  
30  
31  
32  
33  
34  
35  
36  
37  
38  
39  
40  
41  
42  
43  
44  
45  
46  
47  
48  
49  
50  
51  
52  
53  
54  
55  
56  
57  
58  
59  
60

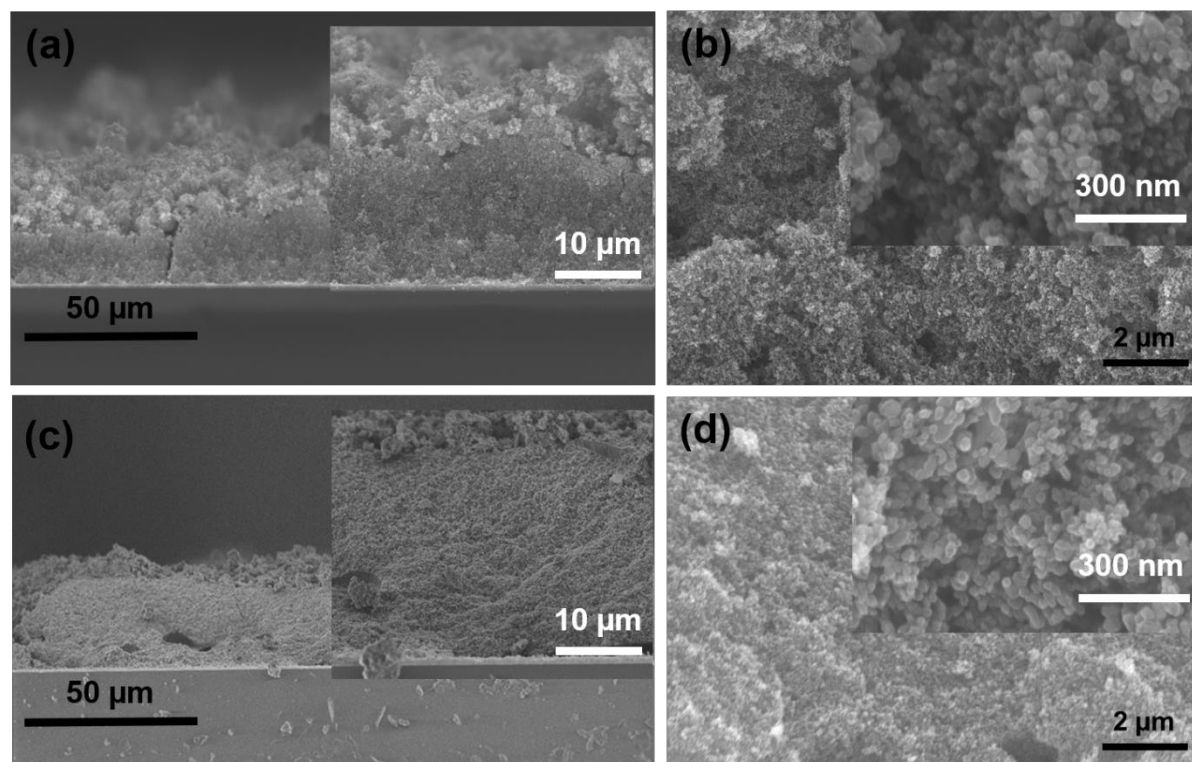


**Figure 7.** Cross-section SEM images of TiO<sub>2</sub> films for (a) day 0 and (c) day 15 aged samples with 45 minute-sonication. The insets in (a) and (c) show the high magnification cross-sections. Top-views of TiO<sub>2</sub> film patterned on FTO-glass substrates for (b) day 0 and (d) day 15 aged samples. The insets in (b) and (d) show the high magnification top-view SEM images.

**Figure 7(a, c)** shows the cross-sectional SEM images of the TiO<sub>2</sub> films prepared after day 0 and day 15, with sonication, respectively. The day 0 TiO<sub>2</sub> film shows weak particle agglomeration that may favor direct contact between the FTO and the electrolyte (**Inset; Figure 7a**). The day 15 sample without sonication shows particles agglomeration whereas the 45-minutes sonicated one shows homogeneously distributed, as revealed in **Figure S1c** and **7c**, respectively. Sonication clearly favored the growth of smooth films, allowing a better interaction between the nanoparticles, which is expected to improve performances. The inset cross-section SEM reveals the formation of uniform and dense TiO<sub>2</sub> film for the day 15 aged sample (**Figure 7c**). Top-view FE-SEM images of TiO<sub>2</sub> films prepared with day 0 and day 15 pastes, with sonication are shown in **Figure 7(b, d)**. Day 0 samples clearly show weak interparticle agglomeration. A non-uniform aggregate of top-view TiO<sub>2</sub> particles is observed

1  
2  
3 in the patterned day 15 paste without sonication (**Figure S1d**). When the TiO<sub>2</sub> paste is  
4  
5 sonicated, the agglomerated particles break down into smaller particles without chemical  
6  
7 dispersants. The inset in **Figure 7d** shows that the TiO<sub>2</sub> film deposited from day 15 paste forms  
8  
9 a smooth film uniformly covering the surface. The reason for the better film formation can be  
10  
11 attributed to the narrow particle size distribution achieved upon ageing of the TiO<sub>2</sub> paste.  
12  
13  
14

### 15 **3.3 TiO<sub>2</sub> Electrodes for Efficient and Reproducible Dye-sensitized Solar Cells**

16  
17  
18 Optimal day 15 for 45 min sonicated TiO<sub>2</sub> paste was used for the DSSC application.  
19  
20 Impact of the ageing of the TiO<sub>2</sub> paste on DSSCs performances was investigated. **Figure S2** is  
21  
22 a schematic illustration of the power-generation mechanism in the TiO<sub>2</sub> electrode based DSSC.  
23  
24 It also highlights the importance of light scattering on the enhancement of light absorption in  
25  
26 the DSSCs. Forward (FS) and reverse (RS) *J–V* scans of the DSSCs made with day 0, and day  
27  
28 15 pastes without and with sonication are presented in **Figure 8a**.  
29  
30  
31  
32  
33  
34  
35  
36  
37  
38  
39  
40  
41  
42  
43  
44  
45  
46  
47  
48  
49  
50  
51  
52  
53  
54  
55  
56  
57  
58  
59  
60

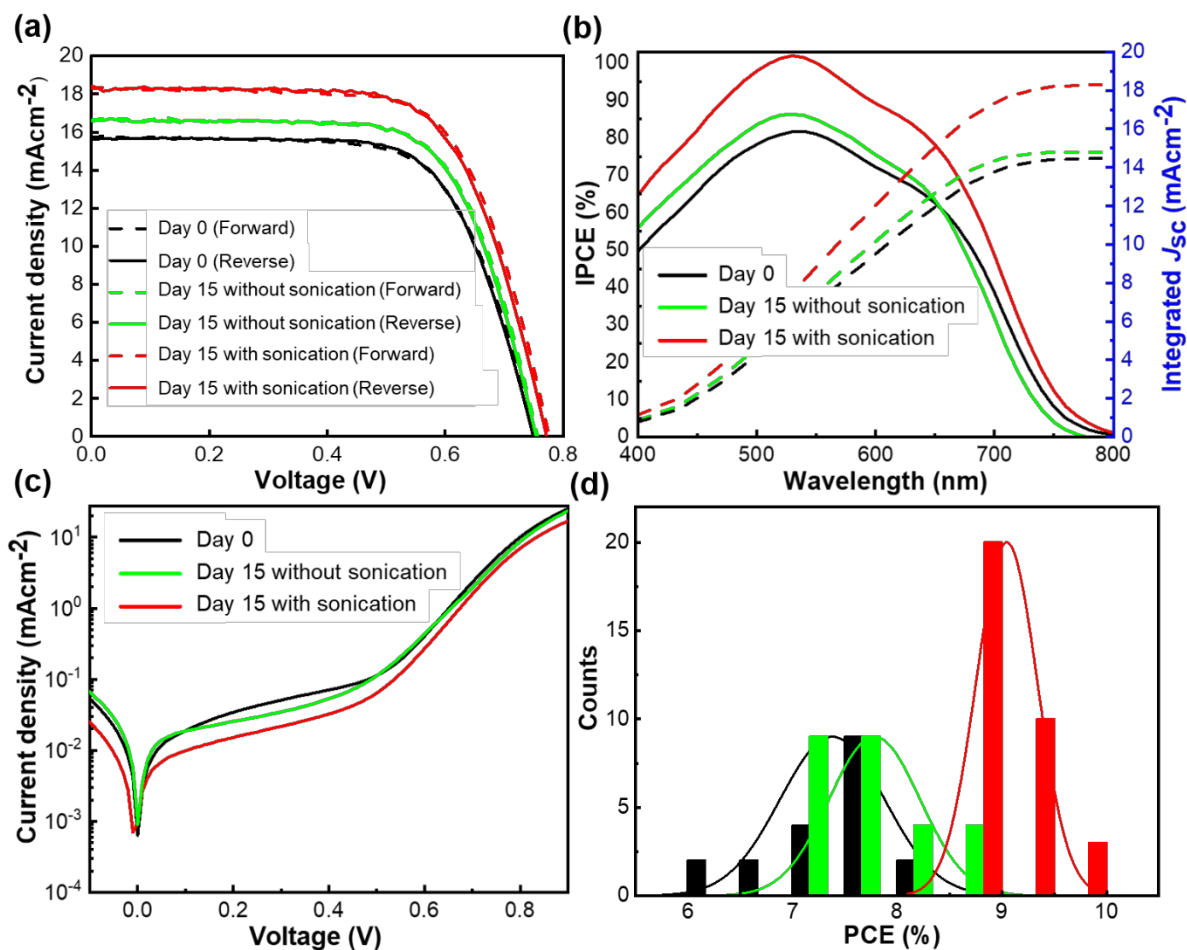


**Figure 8.** (a) Forward scan and reverse scan  $J$ - $V$  curves of DSSCs made with day 0, day 15 with and without sonication, (b) incident photon-to-conversion efficiency (IPCE) spectra with day 0, day 15 with and without sonication, (c) dark  $J$ - $V$  curves for DSSCs with day 0, day 15 with and without sonication, and (d) histogram of PCEs of DSSCs made from day 0, day 15 pastes, with and without sonication.

The photovoltaic characteristics are summarized in **Table 1**, a comparison of the FS and RS results is given in **Table S1**. The day 0 device has a champion PCE of 8.01 %. The poor device performance is attributed to particle-to-particle agglomeration caused by non-uniform aggregates with large voids (**Figure 7a, b**). Sonication breaks the agglomerated particles into smaller ones, which significantly improves device parameters. PCE of the sonicated day 15 DSSC reaches 9.65%, which is larger than the day 15 sample without sonication, and day 0 sample as the photoanode layer (8.68% and 8.01%, respectively). 45 min

sonicated day 15 samples-patterned TiO<sub>2</sub> electrode caused  $J_{sc}$  to increase significantly to 18.3 mAcm<sup>-2</sup>, while it was 16.6 mAcm<sup>-2</sup> for the device without sonication. We attribute this sharp enhancement of  $J_{sc}$  to sonication of the stabilized TiO<sub>2</sub> paste, ensuring stronger particle-to-particle connectivity in a denser scaffold, as evident from SEM (**Figure 7c, d**), thus facilitating electron transport.<sup>47</sup>

**Table 1.** Summary of the parameters of dye-sensitized solar cells made with varying ageing. Statistical analysis (average  $\pm$  standard deviation) was based on the measurement of 19, 26, and 33 individual devices with day 0, day 15 without sonication, and day 15 with sonication, respectively. *Champion* refers to the device with the highest PCE.

TiO <sub>2</sub> electrodes		$J_{sc}$ (mA/cm <sup>2</sup> )	$V_{oc}$ (V)	FF	PCE (%)	Series Resistance (Rs)
Day 0	Champion	15.7	0.75	0.68	8.01	32.75
	Average $\pm$ SD	14.65 $\pm$ 0.9	0.74 $\pm$ 0.02	0.68 $\pm$ 0.01	7.38 $\pm$ 0.5	31.4 $\pm$ 3.53
Day 15 no sonication	Champion	16.6	0.76	0.69	8.68	41.53
	Average $\pm$ SD	15.63 $\pm$ 1.55	0.75 $\pm$ 0.02	0.67 $\pm$ 0.05	7.78 $\pm$ 0.43	38.46 $\pm$ 8.4
Day 15 sonicated	Champion	18.3	0.78	0.68	9.65	27.20
	Average $\pm$ SD	18.39 $\pm$ 0.5	0.74 $\pm$ 0.02	0.66 $\pm$ 0.01	9.05 $\pm$ 0.29	29.02 $\pm$ 2.06

$J_{sc}$  values obtained by integration of the IPCE spectra are 14.5, 14.7 and 18.3 mAcm<sup>-2</sup> for the day 0 day 15 without and day 15 with sonicated paste-based devices, respectively (**Figure 8b**). Values are consistent with the  $J_{sc}$  values extracted from the  $J$ - $V$  curves. The champion DSSC based on day 15 paste has its spectral response extended from the visible to the near-infrared region (approximately 390–780 nm coverage) with a broad, flat absorption peak at ~95%. The wide-ranging IPCE spectrum is attributed to improved light absorption owing to enhanced scattering from the milky TiO<sub>2</sub> electrode, and reduced non-radiative recombination owing to better interconnectivity of the nanoparticles. **Figure 8c** shows that the

day 15 paste with sonication provides a lower dark current density ( $J_{\text{dark}}$ ) than day 0 and day 15 pastes without sonication. A lower dark current density provides a reduced leakage current which is beneficial for  $J_{\text{sc}}$ .<sup>48</sup> It also provides a better rectification which is beneficial to  $V_{\text{oc}}$ , owing to the relation  $V_{\text{oc}} = \frac{kT}{e} \ln \left( \frac{J_{\text{phot}}}{J_{\text{sat}}} + 1 \right)$  which gives the limit of  $V_{\text{oc}}$  under ideal conditions, in which  $k$  is Boltzmann's constant,  $T$  is the temperature,  $e$  is the elementary charge,  $J_{\text{phot}}$  is the photocurrent density and  $J_{\text{sa}}$  is the dark current under large reverse bias.<sup>49</sup> From the data in figure 8, with  $\frac{kT}{e} = 25.7 \text{ meV}$ , it predicts an ideal  $V_{\text{oc}}$  difference of 33 meV, which is consistent with the experimentally measured  $V_{\text{oc}}$  difference between day 0 and day 15 samples. **Figure 8d** shows PCE histogram of each batch of samples with/without sonication. The stabilized day 15 sonicated paste devices exhibit a larger averaged PCE of 9.05% with a narrow distribution from 8.6 to 9.6%. In comparison, day 0 and day 15 pastes without sonication yield averaged PCEs of 7.38% and 7.78%, distributed in a wider range from 6.49 to 8.04% and from 7.17 to 8.68%, respectively. The narrow PCE distribution of the stabilized day 15 sonicated TiO<sub>2</sub> paste devices illustrates the good reproducibility of the processing method. To assess reproducibility of the DSSCs performance, 19, 26, and 33 devices based on day 0, day 15 without and with sonicated pastes were fabricated, respectively. The  $J_{\text{sc}}$ ,  $V_{\text{oc}}$ , FF, and PCE values at compared in **Figure S3**. The day 15 sonicated paste provides superior reproducibility in all photovoltaic parameters than day 0 and day 15 unsonicated-paste samples. A comparison of the best photovoltaic cells PCE based on varying fabrication approaches of TiO<sub>2</sub> electrodes sensitized with N719 dye is given in **Table S2**. To the best of our knowledge, the electro-spray deposited TiO<sub>2</sub> film enabled achieving the highest PCE of 9.65% using the N719 dye sensitization of a TiO<sub>2</sub> photoanode prepared under ambient conditions, among other techniques.

### 3.4 Realization of Multi-Nozzle System for Future Large-scale Solar Modules

1  
2  
3 The single-nozzle approach can typically cover about 5 mm width only. To achieve  
4 large-scale printing with the electro-spray technique, we developed a multi-nozzle system.  
5  
6 When nozzles are set at close distance from each other, the electro-spray printing is not uniform  
7  
8 owing to crosstalk of the electric field around each nozzle. As each nozzle gets isolated from  
9  
10 each other, crosstalk does not happen, and uniform and large-size printing can be achieved.  
11  
12 The proposed electro-spray multi-nozzle set up to print electrodes on flexible or rigid substrates  
13  
14 is illustrated in **Figure S4**. When a high voltage is applied between the nozzles and the FTO-  
15  
16 electrode, small droplets are ejected from the nozzles. Compared to the single-nozzle scheme,  
17  
18 crosstalk between the electric fields of each nozzle results in a higher applied voltage and a  
19  
20 smaller ejection area. Proof of uniformity of small and large-scale electro-spray printing was  
21  
22 provided with a couple of videos. The technique combined with a low-cost fabrication  
23  
24 capability and a high material utilization rate might reduce production cost of the resultant  
25  
26 devices. The multi-nozzle electro-spray technique will be thoroughly explored to coat a variety  
27  
28 of large-scale substrates for high-throughput large-area solar modules in an upcoming study.  
29  
30 Multi-nozzle electro-spray deposited TiO<sub>2</sub> is been provided as a proof of principle for future  
31  
32 large-scale solar modules (**video S2**; Supplementary Information).  
33  
34  
35  
36  
37  
38  
39

#### 40 **4. Conclusions**

41  
42 We tuned the TiO<sub>2</sub> microstructure by ageing the TiO<sub>2</sub> paste for up to 20 days at ambient  
43  
44 atmosphere, which significantly influenced the TiO<sub>2</sub> particle size. DLS evidenced a controlled  
45  
46 TiO<sub>2</sub> particle size, ensuring a dense and uniform microstructure while the TiO<sub>2</sub> paste was aged  
47  
48 between 6 and 20 days. Surprisingly, the paste spontaneously evolved into a higher rutile  
49  
50 content after day 6 and up to day 20, owing to the lower Gibbs energy of the rutile phase. The  
51  
52 nanoparticles also spontaneously stabilized in size. Interestingly, the crystallinity of the as-  
53  
54 deposited day 15 sample evolved spontaneously, without sintering, upon keeping the paste at  
55  
56 ambient condition. Meanwhile, the day 0 sample showed an amorphous structure. The  
57  
58  
59  
60

1  
2  
3 spontaneously improved TiO<sub>2</sub> paste was used to evaluate DSSC's performances. DSSCs made  
4 with the optimized day 15 sonicated TiO<sub>2</sub> paste provide a PCE of 9.65% using the N719 dye.  
5  
6 Revisiting the fabrication procedure of the TiO<sub>2</sub> photoelectrode making use of the spontaneous  
7 evolution of the TiO<sub>2</sub> nano-powder permitted the fabrication of a dense and stable TiO<sub>2</sub>  
8 microstructure, meanwhile maintaining thin-film uniformity across the sample. Green, low-  
9 cost and easily controllable electro-spray is an enabling technology for large-area DSSCs.

## 16 **Associated Content**

### 17 **Supporting Information Description**

21 The Supporting Information is available free of charge on the ACS Publications website  
22 at DOI: Average pore size measured by XRR spectra in TiO<sub>2</sub> films; XRD spectra of TiO<sub>2</sub> films  
23 patterned after sintering on the FTO-substrates for the varying ageing; Cross-section SEM  
24 images of TiO<sub>2</sub> film for samples aged day 15 without sonication, and top-view SEM image of  
25 day 15 without sonication. Schematic of the device architecture. Average of  $J_{sc}$ ,  $V_{oc}$ , FF, and  
26 PCE values of DSSCs made with day 0, day 15 without sonication and day 15 with sonication.  
27 Schematic illustration of the proposed electro-spray multi-nozzles set up. A dense and smooth  
28 TiO<sub>2</sub> electrode was patterned to illustrate the single-nozzle electro-spray technique. Multi-  
29 nozzle electro-spray deposited TiO<sub>2</sub> is been provided as a proof of principle for future large-  
30 scale solar modules.

### 31 **Competing interests**

32 The authors declare no financial and/or nonfinancial interests.

### 33 **Acknowledgements**

34 This study was supported by the Grant-in-Aid for Scientific Research Grant Number  
35 20H02838, 19H02117, 20K20986, and 20H02108. The DLS, XPS and XRD instruments were  
36 supported by the Kagami Memorial Research Institute for Materials Science and Technology  
37 of Waseda University. The FE-SEM was supported by Nanotechnology Research Center of  
38  
39  
40  
41  
42  
43  
44  
45  
46  
47  
48  
49  
50  
51  
52  
53  
54  
55  
56  
57  
58  
59  
60

Waseda University. JMN thanks the Natural Sciences and Engineering Research Council of Canada Discovery Grants program (RGPIN-2020-07016).

### Author Contribution:

M.S. wrote the complete manuscript, drew the figures and supervised the whole study. B.C. conducted the DSSC experiments. M.S, B.C, M.A, L.W, H.F, K.T, S.I, J.M.N., T.T, and S.U. discussed and interpreted the data. J.M.N. wrote partially the manuscript. S.U. designed the ES-experimental setup and supervised the whole study. All authors reviewed and edited the manuscript.

### References

1. Hu, R.; Gong, X.; Duan, Y.; Li, N.; Che, Y.; Cui, Y.; Zhou, M.; Liu, C.; Wang, H.; Hong, F., Neurotoxicological Effects and the Impairment of Spatial Recognition Memory in Mice Caused by Exposure to TiO<sub>2</sub> Nanoparticles. *Biomaterials* **2010**, *31* (31), 8043-8050.
2. Shahiduzzaman, M.; Muslih, E. Y.; Hasan, A. K. M.; Wang, L.; Fukaya, S.; Nakano, M.; Karakawa, M.; Takahashi, K.; Akhtaruzzaman, M.; Nunzi, J.-M.; Taima, T., The Benefits of Ionic Liquids for the Fabrication of Efficient and Stable Perovskite Photovoltaics. *Chem. Eng. J.* **2021**, *411*, 128461.
3. Jacobs, J. F.; van de Poel, I.; Osseweijer, P., Sunscreens with Titanium Dioxide TiO<sub>2</sub> Nanoparticles: A Societal Experiment. *Nanoethics* **2010**, *4* (2), 103-113.
4. Tucci, P.; Porta, G.; Agostini, M.; Dinsdale, D.; Iavicoli, I.; Cain, K.; Finazzi-Agró, A.; Melino, G.; Willis, A., Metabolic Effects of TiO<sub>2</sub> Nanoparticles, a Common Component of Sunscreens and Cosmetics, on Human Keratinocytes. *Cell Death Dis.* **2013**, *4* (3), e549-e549.
5. Iavicoli, I.; Leso, V.; Fontana, L.; Bergamaschi, A., Toxicological Effects of Titanium Dioxide Nanoparticles: A Review of in Vitro Mammalian Studies. *Eur. Rev. Med. Pharmacol. Sci.* **2011**, *15* (5), 481-508.

- 1  
2  
3 6. Shahiduzzaman, M.; Fukaya, S.; Muslih, E. Y.; Wang, L.; Nakano, M.; Akhtaruzzaman,  
4 M.; Karakawa, M.; Takahashi, K.; Nunzi, J.-M.; Taima, T., Metal Oxide Compact Electron  
5 Transport Layer Modification for Efficient and Stable Perovskite Solar Cells. *Materials* **2020**,  
6 *13* (9), 2207.  
7  
8  
9
- 10  
11  
12 7. Zhang, M.; Chen, T.; Wang, Y., Insights into TiO<sub>2</sub> Polymorphs: Highly Selective Synthesis,  
13 Phase Transition, and Their Polymorph-Dependent Properties. *RSC Adv.* **2017**, *7* (83), 52755-  
14 52761.  
15  
16  
17
- 18  
19 8. Zhang, Q.; Gao, L.; Guo, J., Effects of Calcination on the Photocatalytic Properties of  
20 Nanosized TiO<sub>2</sub> Powders Prepared by TiCl<sub>4</sub> Hydrolysis. *Appl. Catal. B.*, **2000**, *26* (3), 207-215.  
21  
22
- 23  
24 9. Han, L.; Islam, A.; Chen, H.; Malapaka, C.; Chiranjeevi, B.; Zhang, S.; Yang, X.;  
25 Yanagida, M., High-Efficiency Dye-Sensitized Solar Cell with a Novel Co-Adsorbent. *Energy*  
26 *Environ. Sci.* **2012**, *5* (3), 6057-6060.  
27  
28  
29
- 30  
31 10. Boschloo, G., Improving the Performance of Dye-Sensitized Solar Cells. *Front. Chem.*  
32 **2019**, *7*, Article 77.  
33  
34
- 35  
36 11. Dubey, R. S.; Jadkar, S. R.; Bhorde, A. B., Synthesis and Characterization of Various  
37 Doped TiO<sub>2</sub> Nanocrystals for Dye-Sensitized Solar Cells. *ACS omega* **2021**, *6* (5), 3470-3482.  
38  
39
- 40  
41 12. Ge, Z.; Wang, C.; Chen, Z.; Wang, T.; Chen, T.; Shi, R.; Yu, S.; Liu, J., Investigation  
42 of the TiO<sub>2</sub> Nanoparticles Aggregation with High Light Harvesting for High-Efficiency Dye-  
43 Sensitized Solar Cells. *Mater. Res. Bull.* **2021**, *135*, 111148.  
44  
45  
46
- 47  
48 13. Shakeel Ahmad, M.; Pandey, A. K.; Abd Rahim, N., Advancements in the Development  
49 of TiO<sub>2</sub> Photoanodes and its Fabrication Methods for Dye Sensitized Solar Cell (DSSC)  
50 Applications. A Review. *Renew. Sustain. Energy Rev.* **2017**, *77*, 89-108.  
51  
52  
53
- 54  
55 14. Krebs, F. C., Fabrication and Processing of Polymer Solar Cells: A Review of Printing and  
56 Coating Techniques. *Sol. Energy Mater. Sol. Cells* **2009**, *93* (4), 394-412.  
57  
58  
59  
60

15. Tsega, M.; Dejene, F. B., Influence of Acidic pH on the Formulation of TiO<sub>2</sub> Nanocrystalline Powders with Enhanced Photoluminescence Property. *Heliyon* **2017**, *3* (2), e00246-e00246.
16. Shimada, K.; Shahiduzzaman, M.; Taima, T., Platinum Leaf Counter Electrodes for Dye-sensitized Solar Cells. *Jpn. J. Appl. Phys.* **2020**, *59* (SD), SDDC07.
17. Shimada, K.; Toyoda, T.; Shahiduzzaman, M.; Taima, T., Platinum Counter Electrodes for Dye-Sensitized Solar Cells Prepared by One-Step Dipping Process. *Jpn. J. Appl. Phys.* **2019**, *58* (12), 124001.
18. Shinde, P. S.; Bhosale, C. H., Properties of Chemical Vapour Deposited Nanocrystalline TiO<sub>2</sub> Thin Films and Their Use in Dye-Sensitized Solar Cells. *J. Anal. Appl. Pyrolysis* **2008**, *82* (1), 83-88.
19. Nejati, S.; Lau, K. K. S., Pore Filling of Nanostructured Electrodes in Dye Sensitized Solar Cells by Initiated Chemical Vapor Deposition. *Nano Lett.* **2011**, *11* (2), 419-423.
20. Anajafi, Z.; Marandi, M.; Taghavinia, N., Hydrothermal Synthesis of TiO<sub>2</sub> Nanocrystals in Different Basic pHs and Their Applications in Dye-Sensitized Solar Cells. *Phys. E: Low-dimens. Syst. Nanostruct.* **2015**, *70*, 113-120.
21. De Marco, L.; Manca, M.; Giannuzzi, R.; Malara, F.; Melcarne, G.; Ciccarella, G.; Zama, I.; Cingolani, R.; Gigli, G., Novel Preparation Method of TiO<sub>2</sub>-Nanorod-Based Photoelectrodes for Dye-Sensitized Solar Cells with Improved Light-Harvesting Efficiency. *J. Phys. Chem. C* **2010**, *114* (9), 4228-4236.
22. Shen, P.-S.; Tseng, C.-M.; Kuo, T.-C.; Shih, C.-K.; Li, M.-H.; Chen, P., Microwave-Assisted Synthesis of Titanium Dioxide Nanocrystalline for Efficient Dye-Sensitized and Perovskite Solar Cells. *Solar Energy* **2015**, *120*, 345-356.
23. Pan, X.; Zhao, Y.; Fan, Z., TiO<sub>2</sub> Nanostructures by Electrochemical Anodization for Dye-Sensitized Solar Cells. *Nanosci. Nanotechnol. Lett.* **2012**, *4* (5), 463-470.

- 1  
2  
3 24. Song, M. Y.; Kim, D. K.; Ihn, K. J.; Jo, S. M.; Kim, D. Y., Electrospun TiO<sub>2</sub> Electrodes  
4 for Dye-Sensitized Solar Cells. *Nanotechnology* **2004**, *15* (12), 1861-1865.  
5  
6  
7  
8 25. Deepak, T. G.; Anjusree, G. S.; Pai, K. R. N.; Subash, D.; Nair, S. V.; Nair, A. S.,  
9 Fabrication of a Dye-Sensitized Solar Cell Module using Spray Pyrolysis Deposition of a TiO<sub>2</sub>  
10 Colloid. *RSC Adv.* **2014**, *4* (44), 23299-23303.  
11  
12  
13  
14 26. Ito, S.; Liska, P.; Comte, P.; Charvet, R.; Péchy, P.; Bach, U.; Schmidt-Mende, L.;  
15 Zakeeruddin, S. M.; Kay, A.; Nazeeruddin, M. K.; Grätzel, M., Control of Dark Current in  
16 Photoelectrochemical (TiO<sub>2</sub>/I<sup>-</sup>-I<sub>3</sub><sup>-</sup>) and Dye-Sensitized Solar Cells. *Chem. Commun.* **2005**,  
17 (34), 4351-4353.  
18  
19  
20  
21  
22  
23  
24 27. Meng, L.; Chen, H.; Li, C.; dos Santos, M. P., Growth of the [110] Oriented TiO<sub>2</sub> Nanorods  
25 on ITO Substrates by Sputtering Technique for Dye-Sensitized Solar Cells. *Front. Chem.* **2014**,  
26 *1*, Article 14.  
27  
28  
29  
30  
31 28. Li, Y.; Ma, L.; Yoo, Y.; Wang, G.; Zhang, X.; Ko, M. J., Atomic Layer Deposition: A  
32 Versatile Method to Enhance TiO<sub>2</sub> Nanoparticles Interconnection of Dye-Sensitized Solar Cell  
33 at Low Temperature. *J. Ind. Eng. Chem.* **2019**, *73*, 351-356.  
34  
35  
36  
37  
38 29. Shahiduzzaman, M.; Sakuma, T.; Kaneko, T.; Tomita, K.; Isomura, M.; Taima, T.;  
39 Umezu, S.; Iwamori, S., Oblique Electrostatic Inkjet-Deposited TiO<sub>2</sub> Electron Transport  
40 Layers for Efficient Planar Perovskite Solar Cells. *Sci. Rep.* **2019**, *9* (1), 19494.  
41  
42  
43  
44 30. Umezu, S.; Kunugi, Y.; Ohmori, H., Dye-Sensitized Solar Cell Utilizing Electrostatic  
45 Inkjet. *Jpn. J. Appl. Phys.* **2013**, *52* (5S1), 05DC23.  
46  
47  
48  
49 31. Davis, T. M.; Drews, T. O.; Ramanan, H.; He, C.; Dong, J.; Schnablegger, H.;  
50 Katsoulakis, M. A.; Kokkoli, E.; McCormick, A. V.; Penn, R. L.; Tsapatsis, M., Mechanistic  
51 Principles of Nanoparticle Evolution to Zeolite Crystals. *Nat. Mater.* **2006**, *5* (5), 400-408.  
52  
53  
54  
55  
56  
57  
58  
59  
60

- 1  
2  
3 32. Rossano, M.; Hucher, N.; Picard, C.; Colletta, D.; Le Foll, F.; Grisel, M., Effects of  
4 Aging on Structure and Stability of TiO<sub>2</sub> Nanoparticle-Containing Oil-in-Water Emulsions.  
5  
6 *International J. Pharm.* **2014**, *461* (1), 89-96.  
7  
8  
9  
10 33. Youn, J.-S.; Park, S.; Cho, H.; Jung, Y.-W.; Jeon, K.-J., Agglomeration Characteristics  
11 of Nano-Size TiO<sub>2</sub> Particles using Analytical Solution. *Korean J. Chem. Eng.* **2018**, *35* (9),  
12 1948-1953.  
13  
14  
15  
16 34. Vemury, S.; Kusters, K. A.; Pratsinis, S. E., Time-Lag for Attainment of the Self-  
17 Preserving Particle Size Distribution by Coagulation. *J. Colloid Interface Sci.* **1994**, *165* (1),  
18 53-59.  
19  
20  
21  
22 35. Hidy, G. M., On the Theory of the Coagulation of Noninteracting Particles in Brownian  
23 Motion. *J. Colloid Sci.* **1965**, *20* (2), 123-144.  
24  
25  
26  
27 36. Segets, D.; Marczak, R.; Schäfer, S.; Paula, C.; Gnichwitz, J.-F.; Hirsch, A.; Peukert,  
28 W., Experimental and Theoretical Studies of the Colloidal Stability of Nanoparticles—A  
29 General Interpretation Based on Stability Maps. *ACS Nano* **2011**, *5* (6), 4658-4669.  
30  
31  
32  
33 37. Penn, R. L.; Oskam, G.; Strathmann, T. J.; Searson, P. C.; Stone, A. T.; Veblen, D. R.,  
34 Epitaxial Assembly in Aged Colloids. *J. Phys. Chem. B* **2001**, *105* (11), 2177-2182.  
35  
36  
37  
38 38. Nakade, S.; Saito, Y.; Kubo, W.; Kitamura, T.; Wada, Y.; Yanagida, S., Influence of  
39 TiO<sub>2</sub> Nanoparticle Size on Electron Diffusion and Recombination in Dye-Sensitized TiO<sub>2</sub>  
40 Solar Cells. *J. Phys. Chem. B* **2003**, *107* (33), 8607-8611.  
41  
42  
43  
44 39. Park, K.; Zhang, Q.; Myers, D.; Cao, G., Charge Transport Properties in TiO<sub>2</sub> Network  
45 with Different Particle Sizes for Dye Sensitized Solar Cells. *ACS Appl. Mater. Interfaces* **2013**,  
46 5 (3), 1044-1052.  
47  
48  
49  
50 40. Hanaor, D. A. H.; Sorrell, C. C., Review of the Anatase to Rutile Phase Transformation. *J.*  
51 *Mater. Sci.* **2011**, *46* (4), 855-874.  
52  
53  
54  
55  
56  
57  
58  
59  
60

- 1  
2  
3 41. Radhakrishnan, T., The Optical Properties of Titanium Dioxide. *Proc. Indian Acad. Sci.-*  
4 *Section A* **1952**, 35 (3), 117.  
5  
6  
7 42. Koo, H.-J.; Park, J.; Yoo, B.; Yoo, K.; Kim, K.; Park, N.-G., Size-Dependent Scattering  
8 Efficiency in Dye-Sensitized Solar Cell. *Inorganica Chim. Acta* **2008**, 361 (3), 677-683.  
9  
10  
11 43. Chiba, Y.; Islam, A.; Watanabe, Y.; Komiya, R.; Koide, N.; Han, L., Dye-Sensitized  
12 Solar Cells with Conversion Efficiency of 11.1%. *Jpn. J. Appl. Phys.* **2006**, 45 (No. 25), L638-  
13 L640.  
14  
15  
16 44. Shahiduzzaman, M.; Kuwahara, D.; Nakano, M.; Karakawa, M.; Takahashi, K.; Nunzi,  
17 J.-M.; Taima, T., Low-Temperature Processed TiO<sub>x</sub> Electron Transport Layer for Efficient  
18 Planar Perovskite Solar Cells. *Nanomaterials* **2020**, 10(9), 1676.  
19  
20  
21 45. Kashiwaya, S.; Morasch, J.; Streibel, V.; Toupance, T.; Jaegermann, W.; Klein, A., The  
22 Work Function of TiO<sub>2</sub>. *Surfaces* **2018**, 1 (1), 73-89.  
23  
24  
25 46. Li, G.; Richter, C. P.; Milot, R. L.; Cai, L.; Schmuttenmaer, C. A.; Crabtree, R. H.;  
26 Brudvig, G. W.; Batista, V. S., Synergistic Effect Between Anatase and Rutile TiO<sub>2</sub>  
27 Nanoparticles in Dye-Sensitized Solar Cells. *Dalton Trans.* **2009**, (45), 10078-10085.  
28  
29  
30 47. Ahmadian-Yazdi, M.-R.; Barratt, C.; Rahimzadeh, A.; Eslamian, M., Microstructural and  
31 Nanostructural Evolution of Light Harvester Perovskite Thin Film under the Influence of  
32 Ultrasonic Vibrations. *ACS Omega* **2020**, 5 (1), 808-821.  
33  
34  
35 48. Ma, J.; Yang, G.; Qin, M.; Zheng, X.; Lei, H.; Chen, C.; Chen, Z.; Guo, Y.; Han, H.;  
36 Zhao, X.; Fang, G., MgO Nanoparticle Modified Anode for Highly Efficient SnO<sub>2</sub>-Based  
37 Planar Perovskite Solar Cells. *Adv. Sci.* **2017**, 4 (9), 1700031.  
38  
39  
40 49. Moliton, A.; Nunzi, J.-M., How to Model the Behaviour of Organic Photovoltaic Cells.  
41 *Polym. Int.* **2006**, 55 (6), 583-600.  
42  
43  
44  
45  
46  
47  
48  
49  
50  
51  
52  
53  
54  
55  
56  
57  
58  
59  
60

1  
2  
3 TOC graphic  
4  
5  
6  
7  
8  
9  
10  
11  
12  
13  
14  
15  
16  
17  
18  
19  
20  
21  
22  
23  
24  
25  
26  
27  
28  
29  
30  
31  
32  
33  
34  
35  
36  
37  
38  
39  
40  
41  
42  
43  
44  
45  
46  
47  
48  
49  
50  
51  
52  
53  
54  
55  
56  
57  
58  
59  
60

